

# Vacancy diffusion in colloidal crystals as determined by dynamical density-functional theory and the phase-field-crystal model

Sven van Teeffelen,<sup>1,\*</sup> Cristian Vasile Achim,<sup>2,†</sup> and Hartmut Löwen<sup>2,‡</sup>

<sup>1</sup>*Department of Molecular Biology, Princeton University, Princeton, New Jersey 08544, USA*

<sup>2</sup>*Institut für Theoretische Physik II, Weiche Materie, Heinrich-Heine-Universität Düsseldorf, D-40225 Düsseldorf, Germany*

(Received 12 October 2012; published 21 February 2013)

A two-dimensional crystal of repulsive dipolar particles is studied in the vicinity of its melting transition by using Brownian dynamics computer simulation, dynamical density-functional theory, and phase-field-crystal modeling. A vacancy is created by taking out a particle from an equilibrated crystal, and the relaxation dynamics of the vacancy is followed by monitoring the time-dependent one-particle density. We find that the vacancy is quickly filled up by diffusive hopping of neighboring particles towards the vacancy center. We examine the temperature dependence of the diffusion constant and find that it decreases with decreasing temperature in the simulations. This trend is reproduced by the dynamical density-functional theory. Conversely, the phase-field-crystal calculations predict the opposite trend. Therefore, the phase-field model needs a temperature-dependent expression for the mobility to predict trends correctly.

DOI: [10.1103/PhysRevE.87.022306](https://doi.org/10.1103/PhysRevE.87.022306)

PACS number(s): 82.70.Dd, 64.70.D-, 81.10.Aj

## I. INTRODUCTION

Most of the mechanical properties of crystals depend crucially on the presence of crystalline defects. For material processing it is therefore of principal importance to understand and control the defect concentration and dynamics. The nature and dynamics of defects are much easier to classify for crystalline sheets in two spatial dimensions. In this case, it has been known for a long time that the formation and unbinding of topological defects provides an efficient way of melting according to the two-stage Kosterlitz-Thouless-Nelson-Halperin-Young (KTNHY) scenario [1]. Defects can also be accumulated near edges of crystalline sheets and do occur for two-dimensional crystals on more complicated manifolds [2,3].

Defects are highly dynamic: Whereas the structure of a crystal is static over long time scales, defects undergo diffusion in the crystalline background. The diffusive dynamics of individual point defects were observed directly in two-dimensional colloidal suspensions of charged microspheres by video microscopy [4,5] and they were confirmed and further analyzed by computer simulations [6]. The dynamics of defects were also explored by real-space methods in a two-dimensional crystal of weakly damped dust particles in a plasma by Nosenko and coworkers [7–9]; see also Ref. [10].

Describing the defect dynamics by a microscopic theory is still a formidable challenge, in particular close to melting. Such a theory should contain the solid and fluid phases and give a reliable picture of the defect concentration and its dynamics. Recent progress in this respect has been made by classical density-functional approaches of freezing [11–14]. For Brownian particles, the density-functional approach can be generalized towards dynamics [15–17] and the dynamics of solidification has been examined in two dimensions [18,19]. Similarly, a more coarse-grained phase-field-crystal model

has been proposed to describe crystal growth [20–23] and the defect structure and dynamics for various applications; see, e.g., Refs. [24–34]. However, a systematic exploration of defect dynamics by such a density-functional theory has not yet been performed nor has the reliability of the phase-field-crystal model been systematically checked as far as the trends of defect dynamics are concerned.

Here, we study the dynamics of vacancies in a two-dimensional colloidal crystal by using Brownian dynamics computer simulations, dynamical density-functional theory, and the phase-field-crystal approach and thereby test the ability of the theoretical approaches to qualitatively reproduce the observations made in the simulations. The model system we use here is a two-dimensional suspension of dipolar colloids. This system has been realized experimentally as superparamagnetic particles at an air-water interface [35]. When exposing superparamagnetic particles to an external magnetic field perpendicular to the plane, their induced magnetic dipole moment leads to an effective repulsive interaction whose amplitude can be tuned by the magnetic field strength. At sufficiently high field strength, the system crystallizes into a two-dimensional triangular (i.e., hexagonal) crystal. This system has been studied extensively by computer simulations and by the aforementioned dynamical density-functional theory [18] and phase-field-crystal models [19].

Out of a perfectly triangular crystal, some particles are removed and the relaxation of the resulting defect and its mobility are extracted by monitoring the one-particle density as a function of time. We confirm by simulation that the defect mobility is increasing with increasing temperature, as was already observed for charged particles by Líbal *et al.* [6]. This behavior is qualitatively and semiquantitatively reproduced in dynamical density-functional theory based on a static Ramakrishnan-Yussouff-like density functional [36,37]. The phase-field-crystal model, on the other hand, fails to predict the trend of the temperature dependence of the mobilities. This is mainly attributed to the constant kinetic prefactor involved in the phase-field-crystal approach. For predicting the trend, a temperature-dependent corrective mobility is needed for the phase-field-crystal model.

\*sven@princeton.edu

†cristian.v.achim@gmail.com

‡hlowen@thphy.uni-duesseldorf.de

This paper is organized as follows: in Sec. II, we briefly propose the different approaches used in this paper. Results are presented in Sec. III and we conclude in Sec. IV.

## II. THEORETICAL MODELS

Dynamical density-functional theory (DDFT) and the more coarse-grained phase-field-crystal model describe the overdamped Brownian dynamics in terms of a continuity equation for the deterministic, time-dependent, and ensemble-averaged one-particle density  $\rho(\mathbf{r}, t)$ . Note that in many applications of the phase-field-crystal model  $\rho(\mathbf{r}, t)$  is interpreted as a fluctuating density field that changes for different realizations of the dynamical evolution even under the same initial conditions. Here, we do not take this approach but regard  $\rho(\mathbf{r}, t)$  as a purely deterministic quantity. For a more thorough discussion of the physical interpretation of  $\rho(\mathbf{r}, t)$  in the phase-field-crystal model, see Refs. [19,38].

The temporal evolution of the density field according to dynamical density-functional theory [15,39] is given by

$$\dot{\rho}(\mathbf{r}, t) = \frac{D}{k_B T} \nabla \cdot \left[ \rho(\mathbf{r}, t) \nabla \frac{\delta F[\rho(\mathbf{r}, t)]}{\delta \rho(\mathbf{r}, t)} \right], \quad (1)$$

with  $D$  being the single-particle diffusion constant and  $k_B T$  being the thermal energy. The Helmholtz free energy functional  $F[\rho(\mathbf{r})]$  is provided by classical density-functional theory [11]. In the crystal, the driving current  $\rho \nabla(\delta F/\delta \rho)$  obviously assumes the hexagonal symmetry of the underlying crystal. In the interstitial regions, this current is small since the density itself is small.

Note that Eq. (1) can be derived from first principles [15,39], i.e., from the microscopic Langevin equations of motion or from the Smoluchowski equation for the time evolution of their respective probability distribution (for a review, see Ref. [19]). Here, we apply the same approximation to the density-functional theory of Ramakrishnan and Yussouff [40] already introduced in Refs. [18,19]. Equation (1) then reads

$$\dot{\rho}(\mathbf{r}, t) = D \left\{ \nabla^2 \rho(\mathbf{r}, t) + (k_B T)^{-1} \nabla \cdot [\rho(\mathbf{r}, t) \nabla V(\mathbf{r}, t)] - \nabla \cdot \left[ \rho(\mathbf{r}, t) \nabla \int d\mathbf{r}' \rho(\mathbf{r}') c_0^{(2)}(|\mathbf{r} - \mathbf{r}'|; \rho) \right] \right\}, \quad (2)$$

where  $V(\mathbf{r}, t)$  is the time-dependent external potential.  $F_{\text{ex}}(\rho)$  and  $c_0^{(2)}(\mathbf{r}; \rho)$  are the excess free energy and the direct correlation function of the reference fluid of density  $\rho$ , respectively.

In this work we consider a two-dimensional (2D) system of magnetic dipoles that are oriented perpendicular to the 2D plane. The pair potential of two dipoles in the plane is given by

$$u(r) = u_0/r^3, \quad (3)$$

where  $u_0$  is the interaction strength. The thermodynamics and structure depend only on one dimensionless coupling parameter  $\Gamma = u_0 \rho^{3/2}/k_B T$ , where  $\rho$  is the average one-particle density and  $k_B T$  is the thermal energy.

The two-particle direct correlation function of the fluid  $c_0^{(2)}(\mathbf{r})$  [41] has been obtained for a large range of coupling constants  $0 < \Gamma \leq 62.5$  from liquid-state integral equation theory as previously described [19,37,42].

In order to measure the diffusion of defects, Eq. (1) is numerically solved on a rectangular periodic box of a fine grid with  $\sim 64$  grid points per nearest-neighbor distance  $a$ . A finite difference method with variable time step is applied. The convolution integrals are solved using the method of fast Fourier transform.

For the more coarse-grained phase-field-crystal model, we employ the two different versions termed PFC1 and PFC2 (phase-field-crystal model versions 1 and 2) in Ref. [19]. The PFC1 model constitutes an approximation of dynamical density-functional theory, as introduced above. The last term in Eq. (2) is replaced by its gradient expansion. The dynamical equation then reads

$$\dot{\rho}(\mathbf{r}, t) = D \nabla^2 \rho(\mathbf{r}, t) + D \nabla \cdot \{ \rho(\mathbf{r}, t) \nabla [(k_B T)^{-1} V(\mathbf{r}, t) - \alpha(\hat{C}_0 - \hat{C}_2 \nabla^2 + \hat{C}_4 \nabla^4) \rho(\mathbf{r}, t)] \}. \quad (4)$$

The parameters  $\hat{C}_0$ ,  $\hat{C}_2$ , and  $\hat{C}_4$  are the fit parameters of a parabola to the first maximum of the Fourier transform of the two-particle correlation function  $\hat{c}_0^{(2)}(k)$ . The coefficient  $\alpha = 1.15$  is artificially introduced to match the melting points of PFC and DDFT.

The second, more coarse-grained model termed PFC2 in Ref. [19], which is frequently used in the phase-field-crystal literature, can be obtained from dynamical density-functional theory by assuming a constant mobility,  $\rho(\mathbf{r}, t) = \rho$  in front of the functional derivative in Eq. (1) and a gradient expansion. The model equation then reads

$$\dot{\phi}(\mathbf{r}, t) = D \rho \nabla^2 [\phi(\mathbf{r}, t) - \frac{1}{2} \phi(\mathbf{r}, t)^2 + \frac{1}{3} \phi(\mathbf{r}, t)^3 + (k_B T)^{-1} V(\mathbf{r}, t) - \alpha \rho (\hat{C}_0 - \hat{C}_2 \nabla^2 + \hat{C}_4 \nabla^4) \phi(\mathbf{r}, t)], \quad (5)$$

with  $\phi(\mathbf{r}, t) = [\rho(\mathbf{r}, t) - \rho]/\rho$  the dimensionless density modulation.

The equation of motion is solved using the finite difference method with a semi-implicit time integration [43].

## III. SETUP AND RESULTS

In the following subsections we qualitatively compare the temperature dependence of defect diffusion as obtained by computational Brownian dynamics simulations and as predicted by the dynamical density-functional theory and the phase-field-crystal model 2 (PFC2).

### A. Brownian dynamics computer simulation

As a reference for the theoretical models we use Brownian dynamics (BD) computer simulations [44] to quantify the diffusion of vacancies for different coupling strengths  $\Gamma$  (well above the melting point at  $\Gamma_m \approx 12$  [45]). Following LÍbal *et al.* [6], we equilibrate a perfectly hexagonal crystal of  $N = 2500$  particles in a rectangular, almost square box, employing periodic boundary conditions while keeping one particle tagged at the origin (see Fig. 1). Subsequently, the particle at the origin is removed and the diffusion of the defect is followed over time. In this setup the vacancy concentration is typically relatively small (of the order  $10^{-3}$ ). The position of the defect is determined by a Voronoi construction: The vacancy appears as one of several configurations of multiple

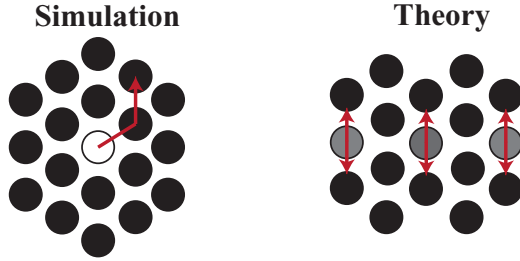


FIG. 1. (Color online) Sketch of the setups in the simulation (left) and theory (right): In the computer simulation we remove one particle out of a perfectly hexagonal lattice and follow the position of the vacancy over time. In dynamical density-functional theory and the phase-field crystal model we study a quasi-one-dimensional relaxation of a depleted central density peak (gray) being replenished by influx of probability density from surrounding density peaks.

particles with more or less than six neighbors (see Fig. 2). The center of mass of these particles is considered as the position of the vacancy.

As was already observed for Yukawa particles in 2D by Lı́bal *et al.* [6], we also find that the defect undergoes diffusion and that the diffusion constant increases with increasing temperature, corresponding to a decreasing coupling strength  $\Gamma$  (Fig. 3). The diffusion constant of the vacancy  $D_V$  ranges between  $18.9(\rho\tau_B)^{-1}$ , for  $\Gamma = 16.6$ , and  $9(\rho\tau_B)^{-1}$ , for  $\Gamma = 28.8$ .

**B. Theory**

In dynamical density-functional theory and in the phase-field-crystal models, crystals appear as strongly modulated density fields that have the symmetry of the corresponding crystal [18,19]. These density fields are mechanically and thermodynamically stable at low temperature or high coupling strength [37]. In an equilibrium density field, the integrated density field over one Wigner-Seitz cell is equal to the probability of finding a particle at the corresponding lattice site. In the approximation to the density-functional theory by Ramakrishnan and Yussouff for magnetic dipoles in 2D described above, this number is very close to 1. A number smaller than 1 can be interpreted as a finite probability of finding a vacancy, and a number larger than 1 can be interpreted as a finite probability of finding an interstitial.

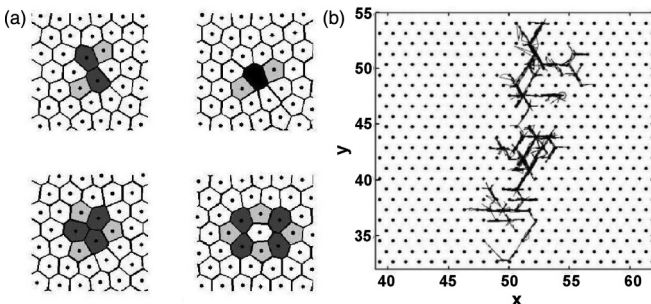


FIG. 2. (a) A vacancy typically appears as one of four different configurations of particles with 5, 7 or 8 neighbors, indicated in light, dark grey and black, respectively. (b) A typical trajectory of a vacancy (similar to results presented in Ref. [6]).

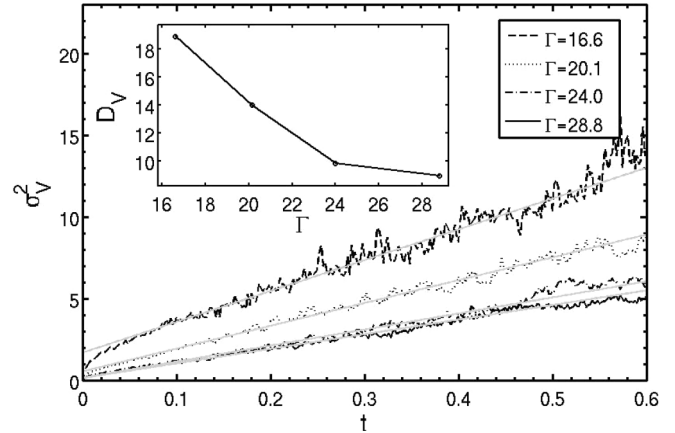


FIG. 3. The mean square displacement for  $\Gamma = 16.6$  (black dashed line),  $\Gamma = 21.12$  (black dotted line),  $\Gamma = 24$  (black dash-dotted line), and  $\Gamma = 28.8$  (black continuous line) obtained from Brownian Dynamics computer simulations. The grey continuous lines are linear fits. Inset: the vacancy diffusion constant  $D_V$ , calculated from the slope of the mean square displacement, as a function of  $\Gamma$ .

Whereas we have addressed the short-time relaxation dynamics of crystals in a previous paper [18], we are here concerned with the long-time dynamics of vacancies. For ease of computation and to assess larger time scales, we thus start with a slightly different setup than the setup in the computer simulations: Instead of introducing a vacancy with probability 1 at the center of a large two-dimensional crystal, which constitutes a problem of cylindrical symmetry, we study the relaxation dynamics of the quasi-one-dimensional setup sketched in Fig. 1: Our reference state is an equilibrium crystalline density field in a periodic rectangular box of dimensions  $L_x \times L_y = 2a \times 64(\sqrt{3}/2)a$ , where  $a$  is the equilibrium lattice constant. At time  $t = 0$  we reduce the integrated density of all density peaks lying on an infinite row of neighboring crystal sites along the  $x$  axis by a small amount of only 3%, thus rendering the problem quasi-one-dimensional (see Fig. 1). Specifically, low-amplitude Gaussians with the same center positions and similar width as the equilibrated density peaks were subtracted from the density field. Thus, the integrated density of each altered peak is smaller by a few percent than its equilibrium value. The temporal behavior of this setup is expected to be qualitatively similar to that of a cylindrical setup at late times, i.e., once the vacancy has diffused a large distance from its initial position.<sup>1</sup> Strictly speaking, the long-time diffusion constant  $D$  should be calculated from the self-part of a van Hove function in the presence of interactions (e.g., by using the test-particle approach to the DDFT [47]). For a low vacancy density, however, the collective and self-dynamics are expected to be similar such that we have avoided the significant additional effort to implement the test-particle approach.

The outcome of the dynamical density-functional theory is summarized in Fig. 4 and based on the  $x$ -averaged density

<sup>1</sup>Ideally one could have started with an initial density profile which describes an ideal single vacancy, but this causes strong numerical problems in the ideal-gas entropy term.

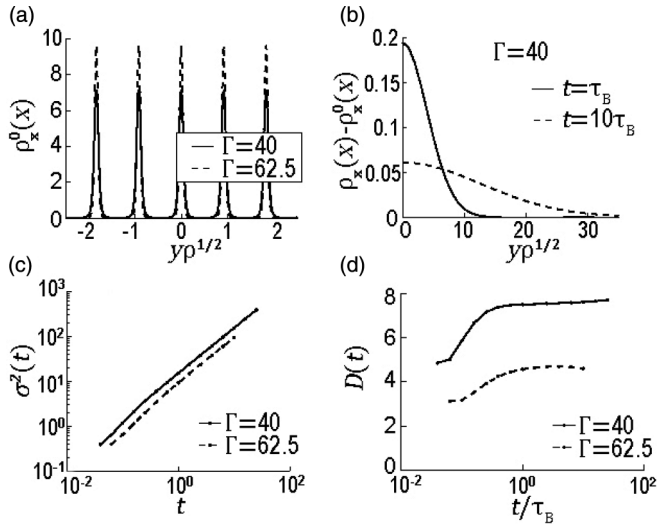


FIG. 4. Results of the dynamical density-functional theory: (a) the initial, equilibrium,  $x$ -averaged density profiles  $\rho_x^0(y,t)$  for two different values of  $\Gamma$ ,  $\Gamma = 40$  and  $\Gamma = 62.5$ , the former being close to the melting point at  $\Gamma = 36$ , (b) the difference of the density profile at time  $t$  and the profile at time 0 measured at the positions of the peaks in panel (a), such that a set of discrete data set is obtained which is in monotonic in  $y$ , (c) the variance  $\sigma^2(t)$  of a Gauss function fitted to panel (b) as a function of time, and (d) the effective diffusion constant calculated as  $D = \sigma_v^2/(2t)$ .

field

$$\rho_x(y,t) \equiv L_x^{-1} \int dx \rho(\mathbf{r},t). \quad (6)$$

Figure 4(a) displays the equilibrium-averaged density field  $\rho_x(y) = \rho_x(y,t=0)$ , i.e., before the introduction of vacancies, for two different coupling strengths,  $\Gamma = 40$  and  $\Gamma = 62.5$ , that are close to and far from the freezing transition at  $\Gamma_f \approx 36$ , respectively.<sup>2</sup> The higher coupling strength corresponds to higher and more pronounced density peaks. Removing a fraction of 0.03 particles from the row of peaks at  $y=0$  leads to restoring density current from neighboring particle rows towards the origin. This is represented by the difference between the  $x$ -averaged density fields of the perturbed and the unperturbed systems at their original  $y$  positions [Fig. 4(b)]:

$$\Delta\rho_x = \rho_x^0(y) - \rho_x(y,t). \quad (7)$$

For small initial perturbations and at long times the envelope of  $\Delta\rho_x$  approaches a Gaussian function, which broadens over time. The variance  $\sigma_v^2(t)$  is plotted in Fig. 4(c). As expected,  $\sigma_v^2(t)$  shows a linear dependence of  $t$  at long times. The long-time slope translates into a diffusion constant given by  $D_v = \sigma_v^2/(2t)$  [Fig. 4(d)]. In agreement with the Brownian dynamics simulations the diffusion constant is higher for low

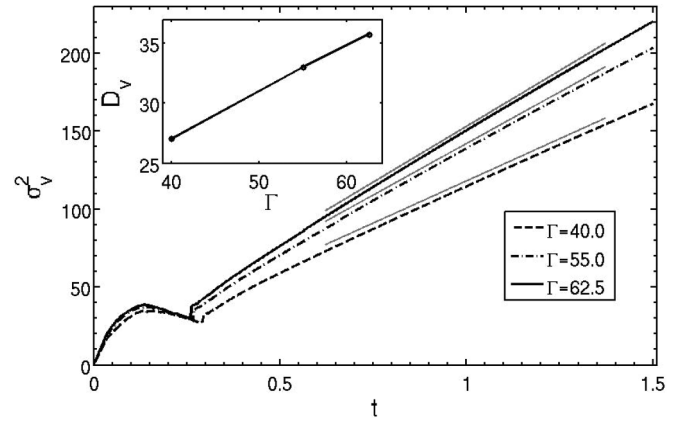


FIG. 5. Results of the PFC2 model: The mean square displacement  $\sigma_v^2$  for  $\Gamma = 40$  (black dashed line),  $\Gamma = 55$  (black dash-dotted line), and  $\Gamma = 62.5$  (black continuous line). The grey continuous lines are linear fits to the curves. Inset: the vacancy diffusion constant  $D_v$ , calculated from the slope of the mean square displacement as a function of  $\Gamma$ .

coupling constant of  $\Gamma = 40$  [ $D_v \approx 7(\rho\tau_B)^{-1}$ ] than for the high coupling constant of  $\Gamma = 62.5$  [ $D_v \approx 4(\rho\tau_B)^{-1}$ ].

The same setup is studied in the PFC1 and PFC2 models. The temporal evolution  $\sigma_v^2(t)$  of the width of the Gaussian envelope function describing the relaxing density field is shown for the PFC2 model in Fig. 5. After a fast transient relaxation process its dependence is linear in time. Remarkably, the corresponding slope  $D_v$  presented in the inset of Fig. 5 is increasing for increasing  $\Gamma$ , in contrast to what has been found before in simulation and DDFT.

The diffusion constant  $D_v$  increases linearly with  $\Gamma$  from  $27(\rho\tau_B)^{-1}$ , corresponding to  $\Gamma = 40$  to  $33(\rho\tau_B)^{-1}$  and  $35.7(\rho\tau_B)^{-1}$  for  $\Gamma$ , equal to 55 and 62.5. The PFC1 model gives the same incorrect trend as the PFC2 models. Again, after a transient process the system reaches a state where the relaxation towards equilibrium is getting diffusive but the slope increases with increasing  $\Gamma$ . The physical reason for the incorrect trend in both variants of PFC models is that the PFC has a smoothed density profile and therefore allows for a quick diffusive current of particles from one lattice site to another. In DDFT, on the other hand, the full density profile is kept and the density decays to very small values in the interstitial region between the density peaks. Thus, particle currents between lattice sites are strongly reduced. For increasing coupling  $\Gamma$ , the interstitial density drops even further down and therefore reduces vacancy diffusion more. This effect is not contained in both PFC models. Here rather the only remaining trend is set by the increasing interactions, which lead to larger interparticle forces and therefore accelerate the dynamics of vacancy diffusion. Therefore, to account for the correct defect dynamics, the temperature dependence of the mobility prefactor in the PFC models needs a proper fitting to reference data. Though this reduces the predictive power of the PFC model, it may still be useful for a fast explorative numerical study for various dynamical effects in solids, provided this fitting is a priori.

<sup>2</sup>We note that while there are large differences between the freezing point  $\Gamma_f$  in DFT and the melting point  $\Gamma_m$  in BD, investigating the fluid-solid transition is beyond the scope of this work. Here we simply quenched the system deep enough into the solid state so that the details of the equilibrium melting process do not matter much.

#### IV. CONCLUSIONS

In conclusion, we have used dynamical density-functional theory, phase-field-crystal theory, and particle-resolved Brownian dynamics computer simulations to calculate the diffusion of defects in a two-dimensional crystal of repulsive dipoles. The typical diffusion coefficient of defect motion is expected to decrease with increasing system temperature as confirmed by the simulation data. This trend is reproduced in the dynamical density-functional theory but not in the phase-field-crystal calculations. These findings show that the PFC model requires a fitting of the kinetic mobilities as a function of the thermodynamic parameters if a realistic description of trends is required to predict material properties. Given the fact that the efficiency of the PFC model is in general achieved by an optimal fitting procedure, also for structural predictions [48], such a phenomenological input of the mobility is an acceptable fact. However, it shows that clearly the dynamical density-functional theory is more appropriate to predict the microscopic time evolution as a first-principle theory for Brownian systems.

Future work should address the dynamics of dipolar mixtures of colloidal particles with different dipole moments [49], where an equilibrium density functional for a binary mixture [50] is needed. These mixtures show more complex

possibilities of mixed crystals as a function of the asymmetry in their dipole moments [51]. In this case one will expect different diffusion coefficients for different defects topologies. Moreover, one should do a similar calculation for hard discs, for which a very accurate functional based on fundamental measure theory [52] was proposed recently [53]. A similar comparison can be performed in three dimensions, e.g., for hard spheres, where the phase-field-crystal model has been tested against density-functional theory recently [48]. Finally it would be interesting to consider particles with orientational degrees of freedom which form liquid crystals with interesting defect structures. In fact, phase-field-crystal models for liquid crystals have been developed [54,55] and applied [56] to freezing recently, which opens the way to describe defect dynamics in liquid crystalline states. An alternative to the usual phase field crystal model is the vacancy PFC model [46]. For the future, it would be interesting to explore defect dynamics within this variant of PFC model.

#### ACKNOWLEDGMENTS

We thank Alexandros Chremos for many useful discussions. This work has been supported by the DFG through the DFG priority program SPP 1296.

- 
- [1] K. J. Strandburg, *Rev. Mod. Phys.* **60**, 161 (1988).
  - [2] A. M. Turner, V. Vitelli, and D. R. Nelson, *Rev. Mod. Phys.* **82**, 1301 (2010).
  - [3] W. T. M. Irvine, V. Vitelli, and P. M. Chaikin, *Nature (London)* **468**, 947 (2010).
  - [4] A. Pertsinidis and X. S. Ling, *Nature (London)* **413**, 147 (2001).
  - [5] A. Pertsinidis and X. S. Ling, *New J. Phys.* **7**, 33 (2005).
  - [6] A. Libál, C. Reichhardt, and C. J. Olson Reichhardt, *Phys. Rev. E* **75**, 011403 (2007).
  - [7] V. Nosenko, G. E. Morfill, and P. Rosakis, *Phys. Rev. Lett.* **106**, 155002 (2011).
  - [8] V. Nosenko, S. K. Zhdanov, A. V. Ivlev, C. A. Knapke, and G. E. Morfill, *Phys. Rev. Lett.* **103**, 015001 (2009).
  - [9] V. Nosenko, S. Zhdanov, and G. Morfill, *Phys. Rev. Lett.* **99**, 025002 (2007).
  - [10] A. V. Ivlev, H. Löwen, G. E. Morfill, and C. P. Royall, *Complex Plasmas and Colloidal Dispersions: Particle-Resolved Studies of Classical Liquids and Solids* (World Scientific, Singapore, 2012).
  - [11] R. Evans, *Adv. Phys.* **28**, 143 (1979).
  - [12] Y. Singh, *Phys. Rep.* **207**, 351 (1991).
  - [13] H. Löwen, *Phys. Rep.* **237**, 249 (1994).
  - [14] H. Emmerich, H. Löwen, R. Wittkowski, T. Gruhn, G. I. Tóth, G. Tegze, and L. Gránásy, *Adv. Phys.* **61**, 665 (2012).
  - [15] U. M. B. Marconi and P. Tarazona, *J. Chem. Phys.* **110**, 8032 (1999).
  - [16] A. J. Archer and R. Evans, *J. Chem. Phys.* **121**, 4246 (2004).
  - [17] P. Español and H. Löwen, *J. Chem. Phys.* **131**, 244101 (2009).
  - [18] S. van Teeffelen, C. N. Likos, and H. Löwen, *Phys. Rev. Lett.* **100**, 108302 (2008).
  - [19] S. van Teeffelen, R. Backofen, A. Voigt, and H. Löwen, *Phys. Rev. E* **79**, 051404 (2009).
  - [20] K. R. Elder, M. Katakowski, M. Haataja, and M. Grant, *Phys. Rev. Lett.* **88**, 245701 (2002).
  - [21] K. R. Elder and M. Grant, *Phys. Rev. E* **70**, 051605 (2004).
  - [22] K. R. Elder, N. Provatas, J. Berry, P. Stefanovic, and M. Grant, *Phys. Rev. B* **75**, 064107 (2007).
  - [23] H. Emmerich, *J. Phys.: Condens. Matter* **21**, 460301 (2009).
  - [24] Y. M. Yu, B. G. Liu, and A. Voigt, *Phys. Rev. B* **79**, 235317 (2009).
  - [25] A. Jaatinen, C. V. Achim, K. R. Elder, and T. Ala-Nissila, *Technische Mechanik* **30**, 169 (2010).
  - [26] C. V. Achim, J. A. P. Ramos, M. Karttunen, K. R. Elder, E. Granato, T. Ala-Nissila, and S. C. Ying, *Phys. Rev. E* **79**, 011606 (2009).
  - [27] J. A. P. Ramos, E. Granato, C. V. Achim, S. C. Ying, K. R. Elder, and T. Ala-Nissila, *Phys. Rev. E* **78**, 031109 (2008).
  - [28] C. V. Achim, M. Karttunen, K. R. Elder, E. Granato, T. Ala-Nissila, and S. C. Ying, *Phys. Rev. E* **74**, 021104 (2006); *J. Phys.: Conf. Ser.* **100**, 072001 (2008).
  - [29] A. Jaatinen, C. V. Achim, K. R. Elder, and T. Ala-Nissila, *Phys. Rev. E* **80**, 031602 (2009).
  - [30] G. Tegze, L. Gránásy, G. I. Tóth, F. Podmaniczky, A. Jaatinen, T. Ala-Nissila, and T. Pusztai, *Phys. Rev. Lett.* **103**, 035702 (2009).
  - [31] Z. F. Huang and K. R. Elder, *Phys. Rev. Lett.* **101**, 158701 (2008).
  - [32] J. Mellenthin, A. Karma, and M. Plapp, *Phys. Rev. B* **78**, 184110 (2008).
  - [33] I. M. McKenna, M. P. Gururajan, and P. W. Voorhees, *J. Mat. Sci.* **44**, 2206 (2009).
  - [34] K. A. Wu and P. W. Voorhees, *Phys. Rev. B* **80**, 125408 (2009).
  - [35] F. Ebert, P. Dillmann, G. Maret, and P. Keim, *Rev. Sci. Instr.* **80**, 083902 (2009).

- [36] F. J. Rogers and D. A. Young, *Phys. Rev. A* **30**, 999 (1984).
- [37] S. van Teeffelen, C. N. Likos, N. Hoffmann, and H. Löwen, *Europhys. Lett.* **75**, 583 (2006).
- [38] A. Archer and M. Rauscher, *J. Phys. A.: Math. Gen.* **37**, 9325 (2004).
- [39] U. M. B. Marconi and P. Tarazona, *J. Phys.: Condens. Matter* **12**, A413 (2000).
- [40] T. V. Ramakrishnan and M. Yussouff, *Phys. Rev. B* **19**, 2775 (1979).
- [41] J.-P. Hansen and I. R. McDonald, *Theory of Simple Liquids*, 3rd ed. (Academic Press, London, 2006).
- [42] S. van Teeffelen, H. Löwen, and C. N. Likos, *J. Phys.: Condens. Matter* **20**, 404217 (2008).
- [43] G. Tegze, G. Bansel, G. I. Tóth, T. Pusztai, Z. Fan, and L. Gránásy, *J. Comput. Phys.* **228**, 1612 (2009); B. P. Vollmayr-Lee and A. D. Rutenberg, *Phys. Rev. E* **68**, 066703 (2003); J. Zhu, L.-Q. Chen, J. Shen, and V. Tikare, *ibid.* **60**, 3564 (1999).
- [44] D. L. Ermak, *J. Chem. Phys.* **62**, 4189 (1975); **64**, 4197 (1975).
- [45] R. Haghgoeie and P. S. Doyle, *Phys. Rev. E* **72**, 011405 (2005).
- [46] P. Y. Chan, N. Goldenfeld, and J. Dantzig, *Phys. Rev. E* **79**, 035701(R) (2009).
- [47] P. Hopkins, A. Fortini, A. J. Archer, and M. Schmidt, *J. Chem. Phys.* **133**, 224505 (2010).
- [48] M. Oettel, S. Dorosz, M. Berghoff, B. Nestler, and T. Schilling, *Phys. Rev. E* **86**, 021404 (2012).
- [49] H. Löwen, E. C. Ögüz, L. Assoud, and R. Messina, *Adv. Chem. Phys.* **148**, 225 (2012).
- [50] T. Kruppa, T. Neuhaus, R. Messina, and H. Löwen, *J. Chem. Phys.* **136**, 134106 (2012).
- [51] L. Assoud, R. Messina, and H. Löwen, *Europhys. Lett.* **80**, 48001 (2007).
- [52] R. Roth, *J. Phys.: Condens. Matter* **22**, 063102 (2010).
- [53] R. Roth, K. Mecke, and M. Oettel, *J. Chem. Phys.* **136**, 081101 (2012).
- [54] H. Löwen, *J. Phys.: Condens. Matter* **22**, 364105 (2010).
- [55] R. Wittkowski, H. Löwen, and H. R. Brand, *Phys. Rev. E* **82**, 031708 (2010).
- [56] C. V. Achim, R. Wittkowski, and H. Löwen, *Phys. Rev. E* **83**, 061712 (2011).